Zhang, Hao; Nakagawa, Hajime

Investigation on Morphological Consequences of Spur Dyke with Experimental and Numerical Methods

INVESTIGATION ON MORPHOLOGICAL CONSEQUENCES OF SPUR DYKE WITH EXPERIMENTAL AND NUMERICAL METHODS

Hao Zhang[1] and Hajime Nakagawa[2]

[1]Assistant Professor, Ujigawa Open Laboratory, Disaster Prevention Research Institute, Kyoto University
Shimomisu, Yoko-oji, Fushimi-ku, Kyoto, 612-8235, Japan, e-mail: zhang@uh31.dpri.kyoto-u.ac.jp
[2]Professor, Ujigawa Open Laboratory, Disaster Prevention Research Institute, Kyoto University
Shimomisu, Yoko-oji, Fushimi-ku, Kyoto, 612-8235, Japan, e-mail: nakagawa@uh31.dpri.kyoto-u.ac.jp

ABSTRACT

The turbulent flow and bed deformation around a single spur dyke is investigated with both experimental and numerical methods. The experiments are conducted under clear-water scour regime with an impermeable or a permeable spur dyke. The scour geometry and flow velocities are measured with a high-resolution laser displacement meter, electro-magnetic velocimetries and PIV (Particle image velocimetry). A 3D morphological model is developed to simulate the complex flow field and scour process. The numerical model is formulated using FVM (Finite volume method) on a collocated unstructured mesh, capable of resolving complex geometries and boundaries. It is found that the simulation results are reasonably consistent with those of the experimental measurements. Based on the study results, the local flow structure and morphological consequences of the spur dyke are characterized.

Keywords: morphological consequence, spur dyke, local scour, 3D numerical model, laboratory experiment

1. INTRODUCTION

Spur dykes are typical in-stream structures in the river engineering to prevent bank erosion, enhance channel navigability, secure water supply, restore channel morphologies and improve aquatic habitats. According to structure permeability, spur dykes are generally categorized into two types: impermeable and permeable. Impermeable spur dykes are built of local soil, stones, gravels, rocks or gabions, while permeable ones (sometimes called pile dykes) usually consist of one or several rows of timber, bamboo, steel or reinforced concrete piles. Protruding of spur dykes to a channel leads to significant changes of flow patterns and bed configurations. These changes bring human either disasters mainly in terms of excessive scouring or benefits such as improvement of channel morphological diversities. Therefore, investigation on the flow and bed deformation around spur dykes is of significant meaning.

Experimental studies on the 3D flow and/or local scour around spur-dyke-like structures have been carried out in several research groups such as Michiue and Hinokidani (1992), Kwan and Melville (1994), Barbhuiya and Dey (2003) and Chrisohoiders et al. (2003). These experiments adopted impermeable spur dyke or similar structures with different shapes. The velocity and bed deformation data may be valuable for understanding the flow nature and be useful for calibration of numerical models. Field measurement data is still very limited. Muto and Baba (2008) investigated the flow field around a series of spur dykes in the Uji River of west Japan with a boat-mounted ADCP (Acoustic Doppler current profiler). Recently, the authors' research group also conducted similar measurements in a large alluvial river: the Jamura River of Bangladesh. For numerical modelling, three kinds of researches have been conducted concerning spur dykes in the past several decades: (1) numerical modeling of flow

field with planar or unscoured bed (e.g. Mayerle et al., 1995; Ouillon and Dartus, 1997; Peng and Kawahara, 1998; Kimura et al., 2002; Chrisohoides et al., 2003 and Ho et al., 2007); (2) numerical modeling of flow field with scoured bed (e.g. Marson et al., 2003; Tominaga and Matsumoto, 2006 and Rasheduzzaman et al., 2007) and (3) numerical modeling of flow field and bed deformation with movable bed (e.g. Bhuiyan et al, 2004; Nagata et al., 2005; Huang, 2006 and Onda et al., 2007). Up to now, it may be concluded that reliable and detailed experiment and/or field data is still insufficient both in amount and in quality concerning the 3D flow and scour geometry around spur dykes. As to numerical models, much space remains to improve the model elaborateness and cost-effectiveness. In order to have a clear image on the morphological consequences of spur dykes, a lot of efforts are needed.

In this paper, fundamental experiments are conducted to investigate the 3D flow structure and local scour in the proximity of an impermeable or a permeable spur dyke. Detailed data of the scour geometry and flow velocity components are collected with high-resolution experimental equipments. An advanced numerical model developed by the authors is used to simulate the complex turbulent flow and the local scour. Based on the research results, different functions of an impermeable and a permeable spur dyke are discussed.

2. LABORATORY EXPERIMENTS

2.1 Experimental setup

Experiments are conducted in a glass-sided tilting flume at the Ujigawa Open Laboratory, Kyoto University. The flume is 8m-long, 40cm-wide and 40cm-deep, with a 1.5m-long inlet tank at upstream (Fig.1). The slope of the flume was adjusted to 1/1000 in the experiments. A working area locates 4m downstream from the inlet tank. It is 1.7m long and is covered with 20cm-thick model sediment. The sediment consists of artificial materials made from sewage sludge ashes. The sediment is almost uniform, having a mean size of d=0.145cm and a specific gravity of s=1.9. The upstream and downstream parts of the working area are fixed with 20cm-thick wooden boards. A 50cm-long sediment trap is set at the end of the flume, followed by a tailgate.

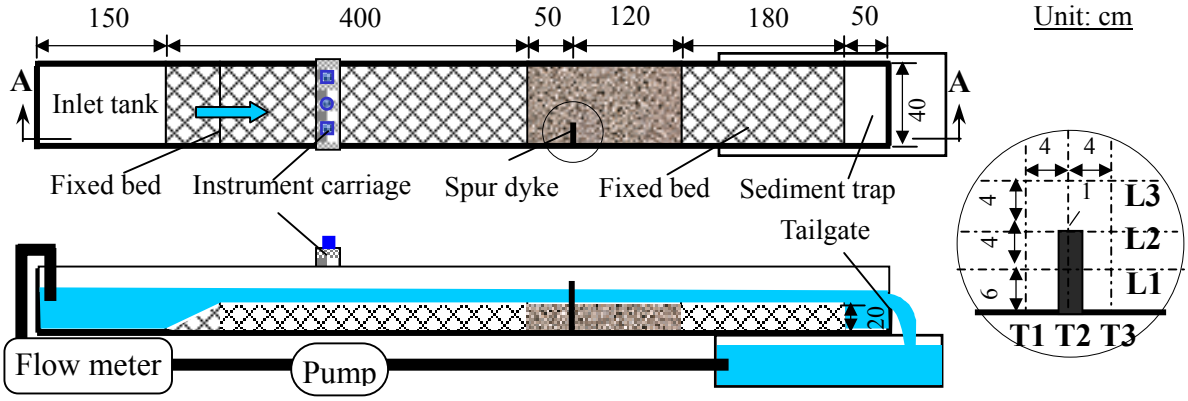

Fig.1 Experimental setup (Plan-view: Top; Section A-A: Bottom; Zoom-in: Right)

A spur dyke is attached to the flume, 1cm-thick and perpendicular to the flume side with a protruding length of 10cm. Two kinds of spur dykes have been tested: impermeable or permeable. The impermeable spur dyke is made of a painted wooden plate, not allowing water passing through it. The permeable one consists of a row of five cuboidal brass piles, having a permeability of 50%.

2.2 Experimental procedure

Before each experiment, the movable bed in the working area was levelled with a scraper blade mounted on a carriage riding on the rails over the model channel. After that, the flume was slowly filled with water from the downstream using a plastic hose. When the desired water depth was achieved by adjusting the height of the tailgate at the end of the flume, the pump was started with the appropriate discharge. The spur dyke was non-submerged in each experiment. Moreover, the scour hole developed under clear-water scour regime. Details of the experimental conditions were summarized in Table 1.

Table 1 Details of the experimental conditions

Discharge	0.0057 m^3/s	Mean diameter of sediment	0.00145 m
Channel slope	1/1000	Specific gravity of sediment	1.9
Channel width	0.4 m	Approaching flow velocity	0.29 m/s
Approach flow depth	0.05 m	u_*/u_{*c}	0.95
Spur dyke length	0.1 m	Reynolds number	14,250
Spur dyke thickness	0.01 m	Froude number	0.41

where u_* = friction velocity and u_{*c} = critical friction velocity.

Local scour developed rapidly in the first several minutes and showed insignificant changes after 1hour in all cases. In this paper, the experiments continued for 2 hours for each case. At the end of each experiment, a point gauge was utilized to measure the water level at some cross-sections. Tracers were distributed in the flume and videos were taken for PIV analysis. Then the pump was stopped. After the flume was completely drained out, a high-resolution laser displacement meter (Model LK-500, Keyence Co., Ltd.) was used to measure the bed deformation. After that, the scoured bed was moulded with instant cement. When the scoured bed was dried, water was pumped into the flume with the same discharge (i.e. 5.7 l/s). The three velocity components at typical cross-sections were then collected using electromagnetic velocimetries with an I-shape or an L-shape probe (Model ACM250-A, Alec Electronics, Co., Ltd). The locations of the measuring cross-sections were shown in Fig.1. At each measuring point, 300 samples were taken at a frequency of 10Hz.

3. NUMERICAL MODELING

3.1 Numerical model

A 3D morphological model was developed to simulate the bed deformation process. The model consists of a hydrodynamic module, a sediment transport module and a bed deformation module.

In the hydrodynamic module, the flow field is obtained with a k-ε model incorporated with the wall-function approach in the near-wall area. The governing equations for the turbulent model are written as

$$\frac{\partial u_i}{\partial x_i} = 0 \tag{1}$$

$$\frac{\partial u_i}{\partial t} + u_j \frac{\partial u_i}{\partial x_j} = f_i - \frac{1}{\rho}\frac{\partial p}{\partial x_i} + \nu \frac{\partial^2 u_i}{\partial x_j \partial x_j} + \frac{1}{\rho}\frac{\partial \tau_{ij}}{\partial x_j} \tag{2}$$

$$\frac{\partial k}{\partial t}+u_j\frac{\partial k}{\partial x_j}=\frac{\partial}{\partial x_j}\left[\left(\nu+\frac{\nu_t}{\sigma_k}\right)\frac{\partial k}{\partial x_j}\right]+G-\varepsilon \tag{3}$$

$$\frac{\partial \varepsilon}{\partial t}+u_j\frac{\partial \varepsilon}{\partial x_j}=\frac{\partial}{\partial x_j}\left[\left(\nu+\frac{\nu_t}{\sigma_\varepsilon}\right)\frac{\partial \varepsilon}{\partial x_j}\right]+\left(C_{1\varepsilon}G-C_{2\varepsilon}\varepsilon\right)\frac{\varepsilon}{k} \tag{4}$$

where t =time; u_i= averaged velocity field; x_i= Cartesian coordinate component; f_i= body force; p= pressure; $\tau_{ij}=-\rho\overline{u_i'u_j'}$, Reynolds stress, where u_i' is the fluctuating velocity field; k= turbulence kinetic energy; ε = dissipation rate of k; G= turbulence production rate; the eddy viscosity $\nu_t=C_\mu k^2/\varepsilon$ and coefficients $C_\mu=0.09$, $\sigma_k=1.0$, $\sigma_\varepsilon=1.3$, $C_{1\varepsilon}=1.44$, $C_{2\varepsilon}=1.92$. When the flow field is resolved, the near-bed shear stress is known, which is a function of the near-bed flow velocity according to the wall-function approach. With the known near-bed shear stress, the flow induced sediment transport rate is obtained with the *Ashida-Michiue* formula (Ashida and Michiue, 1972), which is written as follows

$$\frac{q_b}{\sqrt{(s-1)gd^3}}=17\tau_{*e}^{3/2}\left(1-\sqrt{\frac{\tau_{*c}}{\tau_*}}\right)\left(1-\frac{\tau_{*c}}{\tau_*}\right) \tag{5}$$

where q_b = bedload transport rate per unit width; s = specific gravity of sediment; g = gravitational acceleration; d = sediment diameter; τ_{*e}, τ_{*c}, τ_* = dimensionless effective shear stress, critical shear stress and shear stress, respectively.

The local bed slope may affect the sediment threshold condition as well as the sediment transport rate and direction. Most of the existing literatures account for the bed slope effect under the presumption that the longitudinal flow is predominant and that a bed slope can be treated as a longitudinal slope and a transverse slope separately. Then, a longitudinal bed slope factor and a transverse bed slope factor are introduced correspondingly. For a combined longitudinal and transverse bed, a simple multiplication of these two factors is assumed valid (e.g. van Rijn, 1993 and Duan et al., 2001). Nevertheless, the magnitudes of the velocity components around a spur dyke are usually comparable and the 3D characteristics of the local beds must be preferably considered as a whole. Bearing this in mind, Zhang et al. (2006) suggested a way to consider the bed slope effect based on 3D force analyses of a particle on an arbitrary sloping bed. The basic idea is summarized here and details are referred to Zhang et al. (2006).

Similar to conventional treatments as suggested in van Rijn (1993), a bed slope factor is introduced to express the difference in the critical shear stress between on a sloping bed and on a horizontal bed. After some simplifications and a long derivation process, a new bed slope factor is obtained, which is a function of the local bed slope, angle of sediment repose as well as the near-bed flow velocities. It has been confirmed that conventional bed slope factors as mentioned before are special cases of the new bed slope factor if the longitudinal flow is predominant. The effective shear stress acting on the particle in Eq.5 is a combined contribution from both the near-bed shear stresses and the particle gravity. Furthermore, the sediment transport direction coincides with that of the effective shear stress and is explicitly obtained in the analyses.

When the sediment transport rate is ready, the bed deformation is estimated with the sediment continuity equation in the bedload layer, i.e.

$$(1-\lambda)\frac{\partial z_b}{\partial t}+\left[\frac{\partial q_{bx}}{\partial x}+\frac{\partial q_{by}}{\partial y}\right]=0 \tag{6}$$

where λ = porosity of sediment on the bed and q_{bx} , q_{by} = bedload transport rate in x and y

direction, respectively. With the calculated bed deformation at each mesh, the bed elevation for next time step is easily obtained. Nevertheless, unrealistic local bed slopes over the angle of sediment repose probably occur in the simulation. This phenomenon should be avoided for non-cohesive beds. A sediment slide process is assumed to take place if the local bed slope becomes too steep. After the slide process, the bed level at each mesh is adjusted and all the local bed slopes are no more than the angle of sediment repose. During the adjustment, the mass conservation of sediment must be ensured. Zhang et al. (2006) presented the detailed mathematic expressions.

The well-developed FVM is employed in the model formulation. The governing PDEs (Partial differential equations) are integrated over a number of polyhedral control volumes covering the whole study domain. The integrated equations are then discretized on a collocated unstructured mesh. For reasons of simplicity and stableness, the power law scheme has been adopted during the spatial discretization. The surface fluxes are calculated from the *Rhie-Chow* interpolation method (Rhie and Chow, 1983) in order to avoid the checkerboard phenomenon. In the temporal integral, the second order implicit *Crank-Nicolson* scheme is employed. The widely used SIMPLE (Semi-implicit method for pressure-linked equations) procedure is included for the coupling of the pressure and the velocity. The final algebraic equation systems are solved with a preconditioned GMRES (Generalized minimal residual method) incorporated with an ILUTP (Incomplete LU factorization with threshold and pivoting) preconditioner.

3.2 Computational conditions

Computations were conducted under 4 kinds of conditions varied in terms of types of spur dyke and bed condition as shown in Table 2. Case1 and Case2 simulated the 2-hour bed deformation process from an initial flat bed for impermeable and permeable spur dyke, respectively. Case3 and Case4 were fixed bed simulations for the prediction of flow field based on the scoured bed topography.

Table 2 Simulation cases

Case	Case1	Case2	Case3	Case4
Spur dyke	Impermeable	Permeable	Impermeable	Permeable
Bed condition	Movable bed	Movable bed	Fixed bed	Fixed bed
Time	0-2h	0-2h	Steady	Steady

Hybrid mesh consisting of hexahedra and prisms is used in the simulations. During the mesh generation, a mesh consisting of triangles and quadrilaterals is firstly generated in 2D plane. Then the 2D mesh is extended in the vertical direction according to corresponding water level and bed geometry. A plane view of the mesh system in the neighbourhood of different spur dykes is shown in Fig. 2.

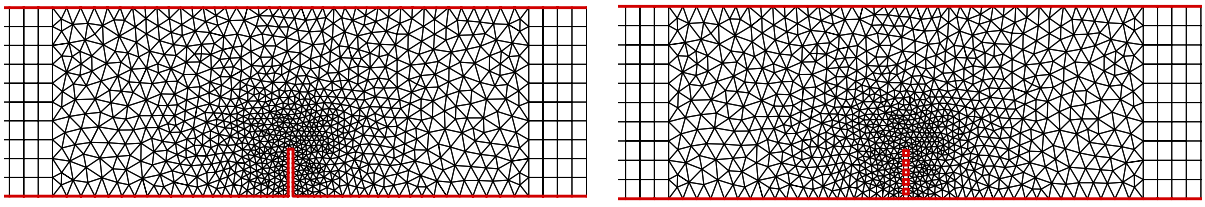

Fig.2 Plan-view of mesh around spur dyke (Impermeable, Left; Permeable, Right)

4 RESULTS AND DISCUSSIONS

4.1 Velocity field

The flow velocities on the free surface are shown in Fig.3 and Fig.4 under the scoured bed conditions for impermeable and permeable spur dykes, respectively.

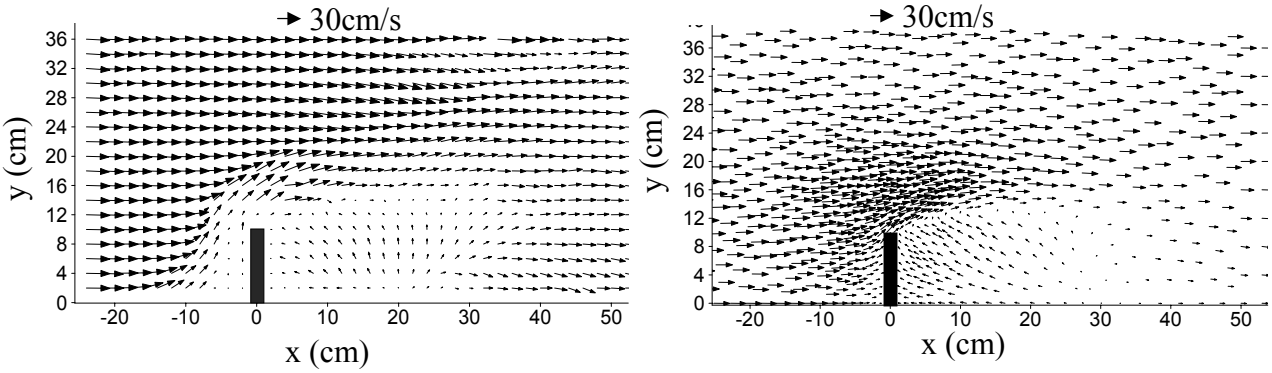

Fig.3 Velocity (*u, v*) on the free surface in impermeable case (PIV, Left; Simulation, Right)

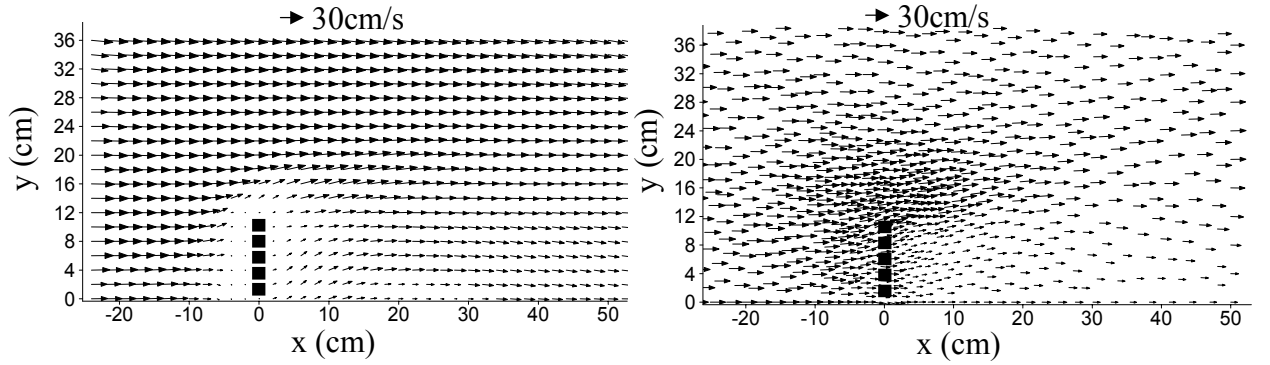

Fig.4 Velocity (*u, v*) on the free surface in permeable case (PIV, Left; Simulation, Right)

If one takes a look at the PIV results in the two figures, one may find some common points of the flow field between the impermeable spur dyke and the permeable one. In both cases, the flow velocities are obviously reduced when the flow approaches and passes the spur dyke. While in the main channel area, the flow velocities are significantly intensified. The wake flow area behind the spur dyke deserves special attention. In the impermeable case, the flow shows a fan-shaped structure. It spreads out from the point (x, y)= (20, 0), which is almost the intersection point of the flume side and the edge of the scour hole. This flow meets the separated flow from the spur dyke head and loses its identity in the mixing zone as described in Zhang and Nakagawa (2008). The fan-shaped flow is a component of a vortex system as will be discussed later. On the other hand, the flow behind the permeable spur dyke does not show significant change in its direction. The differences stem from the local scour geometries and the spur dyke structures themselves. The local flow is complex and highly three-dimensional in impermeable case but is relatively simple and longitudinally dominated in permeable case. Comparing the simulation results with the PIV results, one may find that there are good agreements in most of the flow physics. In the proximity of the spur dyke, it should be mentioned that the PIV data is very little. The flow structure is not well plotted. But in the numerical simulations, the flow structure is very clear. When the flow approaches the spur dyke, it is diverted to the head of the spur dyke in impermeable case but most of the flow passes the spur dyke and a small part is diverted to the head in permeable case. Consequently,

the angles of flow separation are quite different in two cases.

Since the flow in impermeable case is obviously 3D, an investigation on the detailed flow structure is necessary and important to understand the scour process. The velocity profiles at typical longitudinal and transverse sections are hence plotted in Fig.5 and Fig.6.

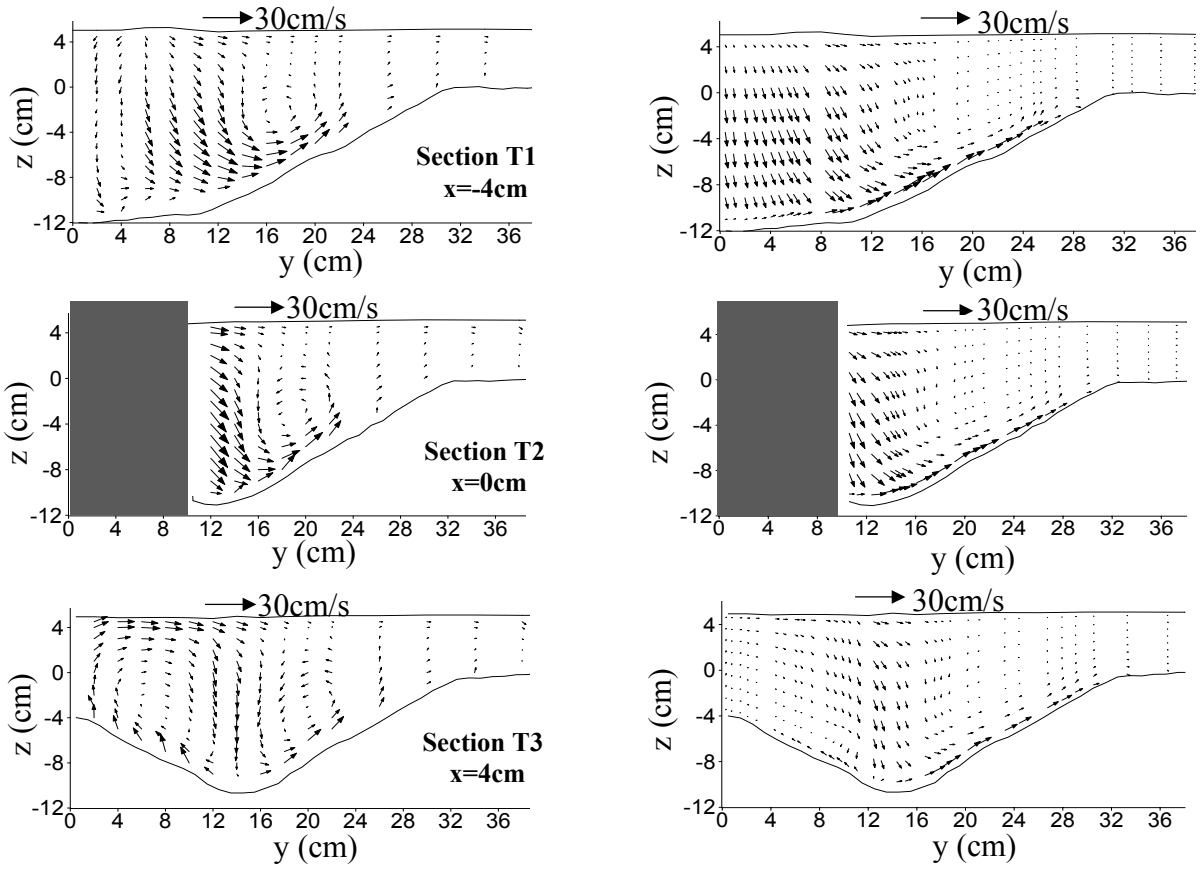

Fig.5 Velocity (*v, w*) at typical transverse sections (Experiment, Left; Simulation, Right)

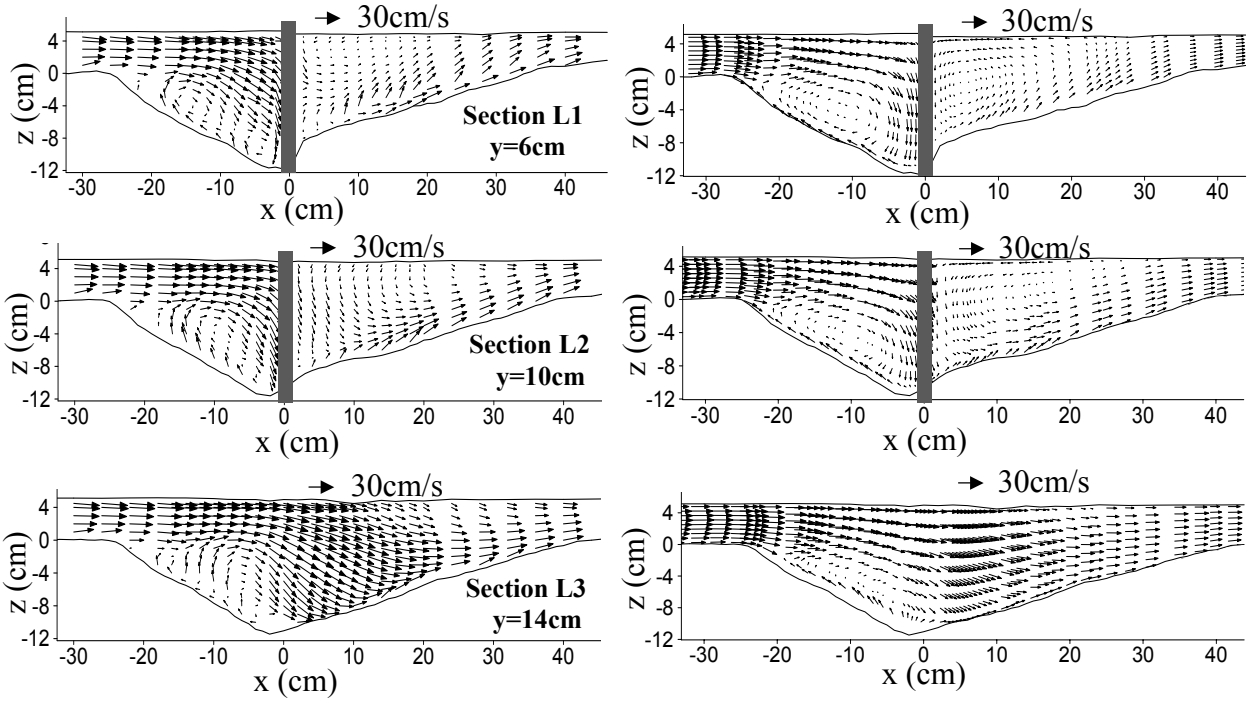

Fig.6 Velocity (*u, w*) at typical longitudinal sections (Experiment, Left; Simulation, Right)

The two major vortices, i.e. the horse-shoe vortex around the head of the spur dyke and the wake vortex behind the spur dyke, are obviously distinguished in both experiments and simulations. There is slight difference between the experimental and numerical results in terms of the magnitudes of the velocity components in some sections. But typical features of the 3D local flow have been reproduced quite well. Taking into account the surface flow structure as shown in Fig.3, one may have a clear picture on the 3D characteristics of the flow field around the impermeable spur dyke.

4.2 Bed deformation

The bed contours at the final stage (2h from the start of each experiment) are shown in Fig.7 and Fig.8. The shape of the local scour in the neighbourhood of either spur dyke is reasonably reproduced with the numerical model. Nevertheless, the predicted maximum scour depth is smaller than that in the experimental measurements. The under-estimation of the velocity components in the scour area as has been mentioned before is the probable reason. Another explanation is the omission of the non-equilibrium transport of sediment around the spur dyke as has been discussed by Michiue and Hinokidani (1992).

Based on both experimental and numerical results, it is found that the maximum scour depth in the impermeable case is more than twice of that in the permeable case. The local scour area in the former case is also much larger than that in the latter one. These differences are caused by the different flow structure and scour mechanism. In permeable case, the local scour is due to the flow separation at the head of the spur dyke and the compressed vortex system in-between two consecutive piles of the spur dyke. While in the impermeable case, the local scour initiates from the flow separation at the spur dyke head. With the development of the scour, two major scour engines, i.e. a horse-shoe vortex and a wake vortex, form in the scour hole as have been shown in the previous context. Scour at spur dyke heads are similar but not identical due to different separation angles. Behind the spur dyke, a long distance of deposition appears in either case due to the significant reduction of flow velocity there.

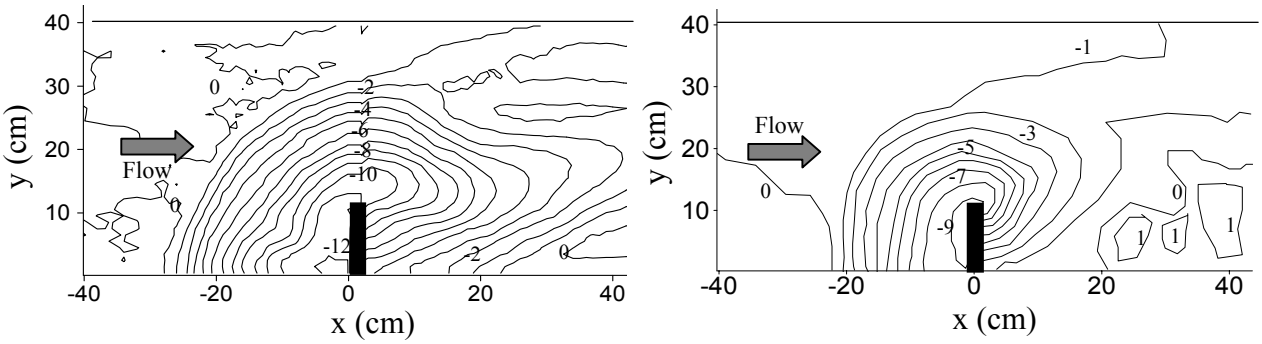

Fig.7 Bed deformation around impermeable spur dyke (Experiment, Left; Simulation, Right)

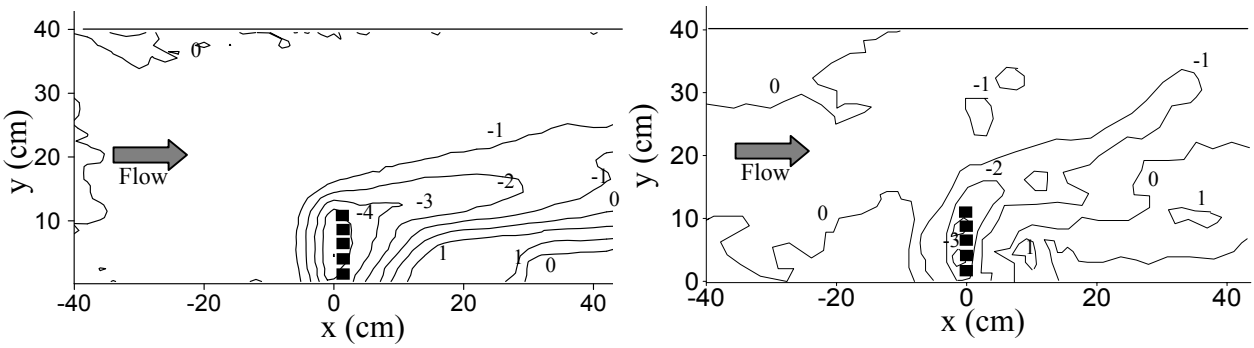

Fig.8 Bed deformation around permeable spur dyke (Experiment, Left; Simulation, Right)

5 CONCLUSIONS

This paper presented a research on the morphological consequences of impermeable and permeable spur dykes with both experimental and numerical methods. The detailed comparisons of the flow field and bed deformation in both impermeable and permeable spur dykes were given. Good agreements were found between the experiments and simulations in terms of both flow field and bed deformation. The impermeable spur dyke had great impacts on the flow structure. The flow velocity was affected in both direction and magnitude, and which resulted in significant local scour around the head of it. The scour gradually extended to the root of the spur dyke. With the development of the scour hole, the 3D characteristics of the flow became more and more evident. The flow structure was generally characterized by several complex vortex systems. The permeable spur dyke reduced the velocity of the flow passing through it. Nevertheless, the direction of the flow velocity was not changed much. Local scour occurred at both the head and the body of the spur dyke. In general, an impermeable spur dyke might be considered as a passive structure and a permeable one was more active. There were some common points concerning the morphological consequences of impermeable and permeable spur dykes. Flow separation was observed around the head of either impermeable spur dyke or permeable spur dyke, although the separation angle was much larger in the former one. The flow separation resulted in similar bed deformation characteristics at the head of different spur dykes. Wake flow zone existed behind the spur dyke in both cases and a long distance of sediment deposition was observed in the downstream of the spur dyke. In order to achieve the maximum beneficial effects and still maintain the effective control of the flow and channel morphology, a combination of impermeable and permeable spur dykes might be suggested. A numerical model, if well calibrated, is a powerful tool to evaluate the morphological consequences of spur dykes in river engineering and river restoration.

ACKNOWLEDGMENTS

This study was supported in part by Toujiro ISHIHARA Research Fellowship from the Association of Disaster Prevention Research, Japan.

REFERENCES

Ashida, K. And Michiue, M., 1972, Studies on bed load transportation for nonuniform sediment and river bed variation, *Annuals of Disaster Prevention Research Institute, Kyoto University*, No. 14B, pp. 259-273 (in Japanese)

Barbhuiya, A. K. and Dey, S., 2003, Vortex flow field in a scour hole around abutments, *International Journal of Sediment Research, WASER*, vol.18, No.4, pp.310-325

Bhuiyan, ABM F., Huque, F. and Saifuddin, AKM., 2004, Numerical modeling of flow pattern and bed evolution around spur-type structures, *Proceedings of the 9th International Symposium on River Sedimentation*, Yichang, China, October 18-21, pp.1497-1502

Chrisohoides, A., Sotiropoulos, F. and Sturm, T. W., 2003, Coherent structures in flat-bed abutment flow: computational fluid dynamics simulations and experiments, *Journal of Hydraulic Engineering, ASCE*, vol.129, No.3, pp.177-186

Duan, J.G., Wang, S.S.Y. and Jia, Y., 2001, The application of the enhanced CCHE2D model to study the alluvial channel migration processes, *Journal of Hydraulic Research, IAHR*, vol.39(5), pp. 1-12

Ho, J., Yeo, H. K., Coonrod, J. and Ahn, W. S., 2007, Numerical modeling study for flow pattern changes induced by single groyne, *32nd Congress of IAHR*, Venice, Italy, July 1-6, CD-ROM

Huang, G. X. 2006, Study on the three-dimensional numerical simulation of fluvial processes in meandering and braided channel, *Doctoral Thesis, Tsinghua University*, Beijing (in Chinese)

Kimura, I., Hosoda, T. and Onda, S., 2002, Prediction of 3D flow structures around skewed spur dikes by means of a non-linear *k-ε* model, *River Flow 2002*, Bousmar & Zech (eds), Balkema, vol.1, pp.65-73

Kwan, R. T. F. and Melville, B. W., 1994, Local scour and flow measurements at bridge abutments*, Journal of Hydraulic Research, IAHR*, vol.32, No.5, pp.661-674

Marson, C., Caroni, E., Fiorotto, V. and Da Deppo, L., 2003, Flow field analysis around a groyne, *31st IAHR Congress*, Thessaloniki, Greece, August 24-29, vol.2, pp.377-384

Mayerle, R., Toro, F. M. and Wang, S. S. Y., 1995, Verification of a three-dimensional numerical model simulation of the flow in the vicinity of spur dikes, *Journal of Hydraulic Research, IAHR*, vol.33, No.2, pp.243-256

Michiue, M. and Hinokidani, O., 1992, Calculation of 2-dimensional bed evolution around spur-dike, *Annual Journal of Hydraulic Engineering, JSCE*, vol.36, pp.61-66 (in Japanese)

Muto, Y. And Baba, Y. (2008), Secondary flow measurements in a river by a boat-mounted ADCP, *Annual Journal of Hydraulic Engineering, JSCE*, Vol. 52, pp. 925-930 (in Japanese)

Nagata, N., Hosoda, T., Nakato, T. and Muramoto, Y., 2005, Three-dimensional numerical model for flow and bed deformation around river hydraulic structures, *Journal of Hydraulic Engineering, ASCE*, vol.131, No.12, pp.1074-1087

Onda, S., Hosoda, T., Kimura, I. and Iwata, M., 2007, Numerical simulation on local scouring around a spur dyke using equilibrium and non-equilibrium sediment transport models, *Annual Journal of Hydraulic Engineering, JSCE*, vol.51, pp.943-948 (in Japanese)

Ouillon, S. and Dartus, D., 1997, Three-dimensional computation of flow around groyne, *Journal of Hydraulic Engineering, ASCE*, vol.123, No.11, pp.962-970

Peng, J. and Kawahara, Y. 1998, Application of linear and non-linear k-εmodels to flows around spur dykes, *Annual Journal of Hydraulic Engineering, JSCE*, vol.42, pp.643-648

Rasheduzzaman, M., Nakagawa, H., Zhang, H., Rahman, Md. M. and Muto Y., 2007, Flow and sediment transport around bandals under live-bed scour condition, *Annual Journal of Hydraulic Engineering, JSCE*, Vol.51, pp. 145-150

Rhie, C.M. and Chow, W.L. 1983, Numerical study of the turbulent flow past an airfoil with trailing edge separation, *Journal of AIAA*, Vol. 21, pp. 1525-1532

Tominaga, A. and Matsumoto, D. 2006, Diverse riverbed figuration by using skew spur-dike groups, *River Flow 2006*, Ferreira, Alves, Leal & Cardoso (eds), Taylor & Francis Group, pp.683-691

Van Rijn, L.C., 1993, *Principles of Sediment Transport in Rivers, Estuaries and Coastal Seas*, AQUA Publications, Amsterdam, the Netherlands

Zhang, H. and Nakagawa, H., 2008, Scour around spur dyke: recent advances and future researches, *Annuals of the Disaster Prevention Research Institute, Kyoto University*, No. 51B, 20p

Zhang, H., Nakagawa, H., Muto, Y., Baba, Y. and Ishigaki, T., 2006, Numerical simulation of flow and local scour around hydraulic structures, *River Flow 2006*, Ferreira, Alves, Leal & Cardoso (eds), Taylor & Francis Group, pp.1683-1693